From steady solutions to chaotic flows in a Rayleigh–Bénard problem at moderate Rayleigh numbers

Carles Simó

Dept. Matemàtica Aplicada i Anàlisi, UB, Barcelona, Catalunya

carles@maia.ub.es

Dynamic Days 2012

Session on Global bifurcations: dynamics associated to cycles

Benicàssim, Castelló, València, 1210241600

Joint work with Dolors Puigjaner, Joan Herrero and Francesc Giralt, URV

(see Physica D, 240, (2011), 920–934)

Contents

- **The physical problem and motivations**
- **The equations of the problem**
- **What we want to do: why and how**
- **A short comment on the numerical methods**
- **Results: Some bifurcation diagrams, related to steady solutions, to some periodic orbits and to the creation of chaos**
- **Chaotic dynamics**
  - **Chaotic dynamics at** $Pr = 0.71$
  - **Chaotic attractors at** $Pr = 0.75$ **and** $Pr = 0.80$

Introduction to the problem

Goal: to study the **dynamics of a Rayleigh–Bénard convection** problem. To **understand different dynamical mechanisms**.

This is the dynamics in a **bounded domain** created by **differences of temperature** between the walls.

One of the most difficult problems is the case of a **cubical cavity** due to **multiplicities** because of the symmetries.

For concreteness the cubical domain is assumed to be **heated from below** with **perfectly conducting sidewalls** and **uniform temperature at the top and bottom** walls.

The main **physical parameters** are **Rayleigh and Prandtl** numbers. Our goal is to give **strong evidence** that **chaotic dynamics and chaotic attractors exist** at **moderate Rayleigh numbers**.

A realistic **motivation** is to have **enhanced mixing** properties in small domains where a **chemical reaction is made possible by the presence of some bacterias**. Their presence prevents from **large temperature changes**.

The equations

We assume the cube to be of **side** L and normalised to $\Omega = [-1/2, 1/2] \times [-1/2, 1/2] \times [-1/2, 1/2]$ with **top and bottom temperatures** T_c **and** T_h**,** $T_c < T_h$**,** $\Delta T = T_h - T_c$.

Physical parameters:

ρ = density, β = thermal expansion, α = thermal conductivity, ν = kinematic viscosity, g = gravity acceleration. Then the Rayleigh, Ra, and Prandtl, Pr, numbers are defined as

$$Ra = \beta(\Delta T) g L^3/\alpha\nu, \qquad Pr = \nu/\alpha.$$

The **main parameter to change is** Ra for a **fixed** Pr. Most of the computations will be done with $Pr = 0.71$ **(air at 300 K)**.

Later on it will be **necessary for our purpose** to change the value of Pr. The values $Pr = 0.75$ **(CO_2 at 380 K)** and $Pr = 0.80$**, (butane at 300 K)**, will be used.

For the presentation of some results we shall use the **Nüsselt number** Nu, that is, the dimensionless **convective heat transfer coefficient** at the hot bottom wall. Nu_a **is the averaged** value of Nu for an amount of time, to be taken equal to **the period** in the case of p.o.

In most of the plots Nu is replaced by the **modified value** $Nu - 0.012 Ra^{1/2}$ for plot clarity.

Variables:

The velocity $\mathbf{V} = (u, v, w)$, **temperature departure** from the linear motionless conductive state θ and the **pressure** p. Then we have

$$Pr^{-1}\left(\frac{\partial \mathbf{V}}{\partial t} + Ra^{1/2}(\mathbf{V}\cdot\nabla)\mathbf{V}\right) - \nabla^2\mathbf{V} - Ra^{1/2}\theta\,\mathbf{e}_z + \nabla\, p = 0$$

$$\frac{\partial \theta}{\partial t} + Ra^{1/2}(\mathbf{V}\cdot\nabla)\theta - \nabla^2\theta - Ra^{1/2}w = 0\,, \qquad \nabla\cdot\mathbf{V} = 0.$$

The **boundary conditions** are

$$u = v = w = \theta = 0 \textbf{ along } |x| = 1/2,\ |y| = 1/2,\ \textbf{and } |z| = 1/2.$$

The equations are **adimensionalised** taking suitable units and are written using the **vorticity**, so that instead of $(\mathbf{V} \cdot \nabla)\mathbf{V}$ appears $\omega = \nabla \times \mathbf{V}$ and instead of ∇p appears $\nabla \Pi$ where $\Pi = p + |\mathbf{V}|^2/2$.

Symmetries

$$
\begin{array}{llll}
S_x & : (x,y,z) \to (-x,y,z)\,, & & (u,v,w,\theta) \to (-u,v,w,\theta)\,, \\
S_y & : (x,y,z) \to (x,-y,z)\,, & & (u,v,w,\theta) \to (u,-v,w,\theta)\,, \\
S_z & : (x,y,z) \to (x,y,-z)\,, & & (u,v,w,\theta) \to (u,v,-w,-\theta)\,, \\
S_{d_+} & : (x,y,z) \to (y,x,z)\,, & & (u,v,w,\theta) \to (v,u,w,\theta).
\end{array}
$$

These elements generate the **symmetry group** $D_{4h} = \mathbb{Z}_2 \times D_4$ where $\mathbb{Z}_2$ is generated by the **reflection** about the horizontal midplane, S_z, and D_4 is the **dihedral group** generated by S_y and S_{d_+}. These symmetries are responsible for the existence of **multiple invariant subspaces** in the space of solutions of the equations.

There are **solutions invariant under some subgroup of** D_{4h}. We denote these subgroups as G_i. They **leave invariant a subspace, denoted as** E_i. In particular we shall make **strong use of** G_7**, generated by** $-S_z = -I \cdot S_z$, i.e., a rotation by π around the z-axis, and **leaving invariant** E_7. The **full space is denoted as** E_0 (G_0 generated by I).

What we want to do, why and how

What: We want to obtain, **in a moderate range of Ra** the **skeleton of the dynamics**, that is, the different **invariant objects, like steady state solutions, periodic orbits, their stability properties and some invariant manifolds**.

Why: As said at the Introduction we look for **the existence of chaotic dynamics and chaotic attractors** for moderate values of Ra.
Another motivation is **to realise that techniques used typically in low dimensional dynamical systems** can be applied systematically to **infinite dimensional ones**.
An additional motivation is **to stress the importance of following unstable solutions**. They can **become stable** and attract the dynamics or **be involved in homoclinic/heteroclinic phenomena** leading to **chaotic dynamics**.

How: We use **numerical tools** guided by the **knowledge on dynamical systems**. We give an **interpretation of the results concerning the dynamics**.

A short comment on the numerical methods

The equations are **discretised in space** by means of a **Galerkin** spectral method with a complete **divergence–free** set of basis functions. The velocity and temperature fields are approximated by

$$\begin{pmatrix} \mathbf{V} \\ \theta \end{pmatrix}(t,x,y,z) = \sum_{i=1}^{n}\sum_{j=1}^{n}\sum_{k=1}^{n}\sum_{l=1}^{4} c_{ijk}^{(l)}(t)\mathbf{F}_{ijk}^{(l)}(x,y,z)\,,$$

where $c_{ijk}^{(l)}(t)$ are the **unknown time–dependent coefficients**, and $F_{ijk}^{(l)}(x,y,z)$ are the **basis functions**.

Typically **n=14** has been used. Hence the number of **unknown coefficients amounts to** $N = 14^3 \times 4 = 10976$. For **checks** values like $n = 12$ ($N = 6912$) or $n = 16$ ($N = 16384$) have been used. The **symmetry** of some solutions **reduces the number of unknowns** in some cases.

The **set of ODE** obtained can be represented in matrix form as

$$B\,d\mathbf{x}/dt = (L_1 + \lambda L_2)\,\mathbf{x} + \lambda Q(\mathbf{x},\mathbf{x})\,, \qquad \lambda = Ra^{1/2},$$

where $\mathbf{x}$ are the **coefficients**, B, L_1 and L_2 are **linear operators** and Q is a **quadratic operator**.

A list of tools:

- **Computation of steady states** (fixed points) and its **stability**,
- **Computation of periodic solutions** and its **stability**. As in the previous case **Newton-Krylov** methods are used,
- **Continuation of solutions** via **arc-length** and variants,
- **Detection of bifurcations** in both cases,
- **Computation of invariant unstable manifolds** for the **flow or suitable Poincaré maps**,
- **Detection/computation of homoclinic and heteroclinic** connections,
- **Computation of the relevant Lyapunov exponents**,
- **Multiple checks** using **different values of** n, different **time integration steps**, different ways to **evaluate the quadratic terms**, many **random initial conditions** and several **long time integrations**.

A sample of results

Next we shall show some **bifurcation diagrams of steady state and periodic solutions**. For other **diagrams**, the **symmetries** of the different solutions (if any), numerical values of the **ranges of stability** and **illustrations** for other kinds of orbits, see the paper.

Notation: Steady solutions bifurcating from the motionless state are **labelled as B_i**. In **subsequent bifurcations** appear the ones labelled $B_{ij}, B_{ijk}, \ldots$. **Similar notation for periodic orbits**: $po_jB_i, po_{jk}B_i$, po_kB_{ij}, etc. This allows to follow the **genealogy** of the different families.

The steady solutions **not bifurcating from the motionless state** are labelled as A_i. They appear by **fold (SN) bifurcation**.

Typically **stable (unstable)** solutions shown with solid (dashed) lines.

For **steady state** solutions **pitchfork (Hopf)** bifurcations are marked with **filled (hollow) circles**,

For **periodic** solutions
Filled circles, squares, triangles $\Longrightarrow$ pitchfork, homoclinic and Neimark-Sacker.
Hollow circ., squa., triang. $\Longrightarrow$ Hopf, fold and period doubling.

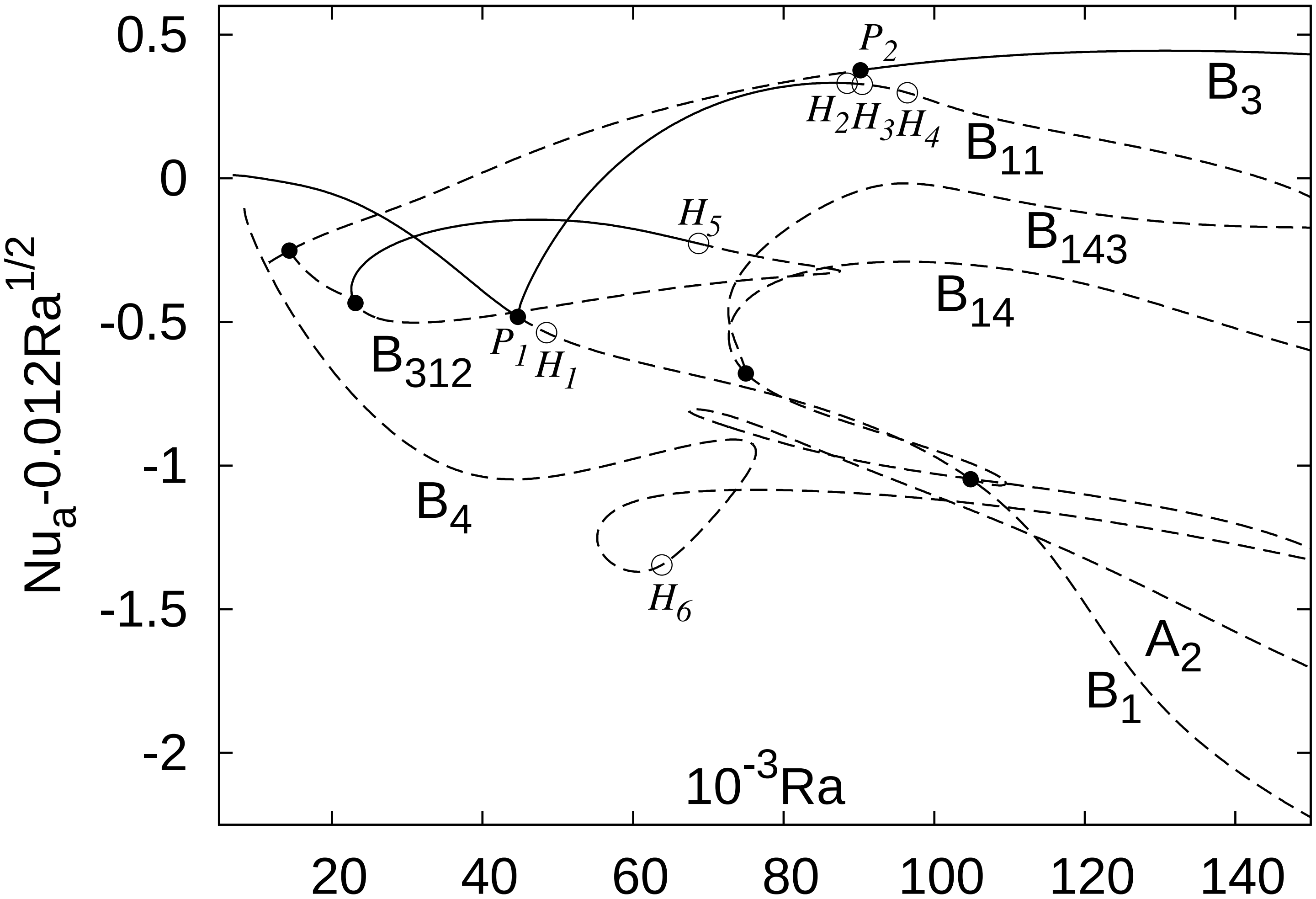

Bifurcation diagram of the **steady solutions** B_1, B_3, B_4, A_2, B_{11}, B_{14}, B_{312} and B_{143} for $Pr = 0.71$.

The branches B_1, B_3 and B_4 are born at the **basic conductive state** at $Ra = 6\,799$, $11\,612$ and $8\,353$ respectively.

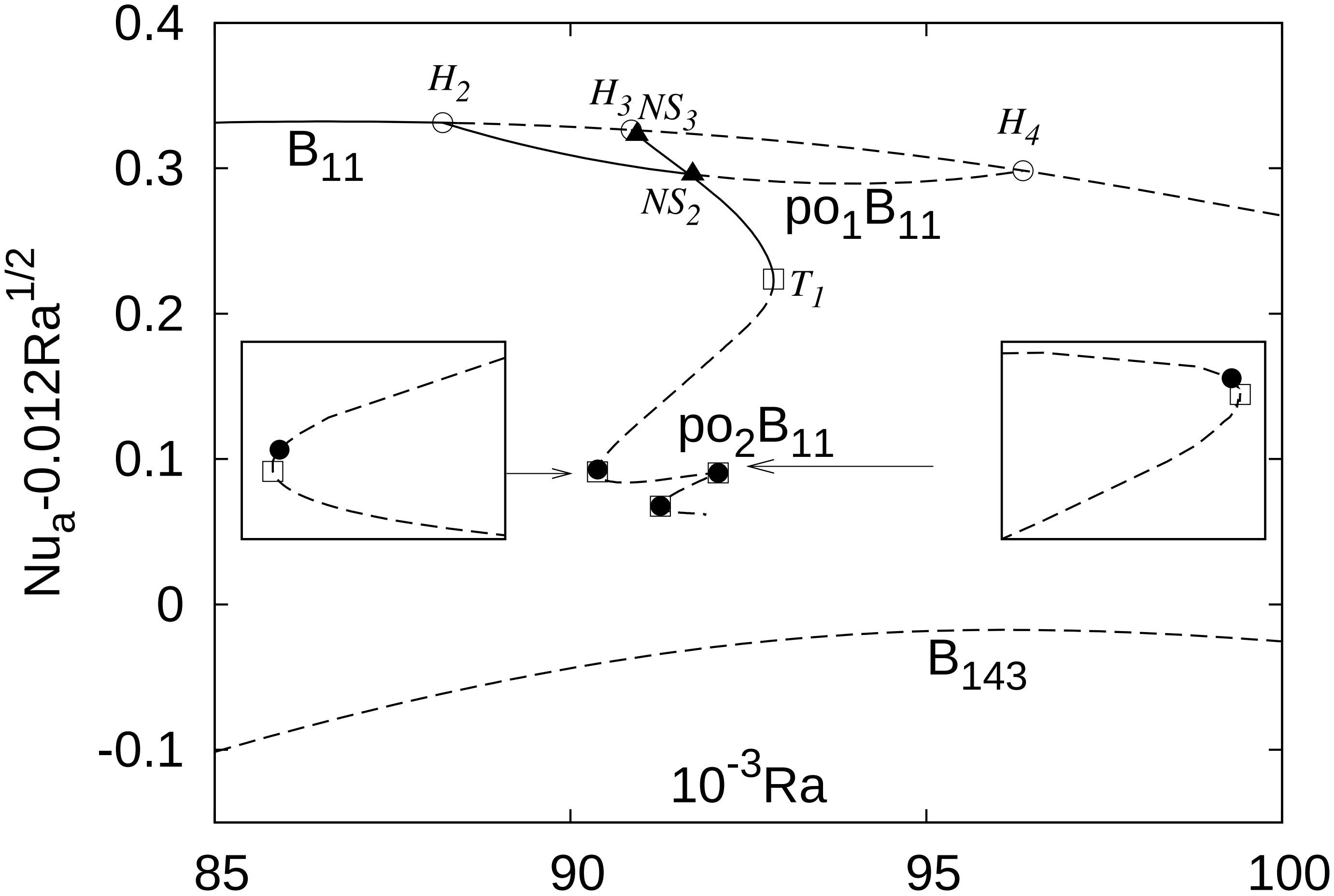

Bifurcation diagram of periodic orbits related to the B_{11} solution. Note that the po_1B_{11} and po_2B_{11} branches **do not intersect near** NS_2. It is due to the projection. po_1B_{11} **joints** H_2 **to** H_4 and **loses stability at** NS_2.

po_2B_{11} **starts unstable at** H_3 and becomes **stable at** NS_3. It **loses stability** at T_1.

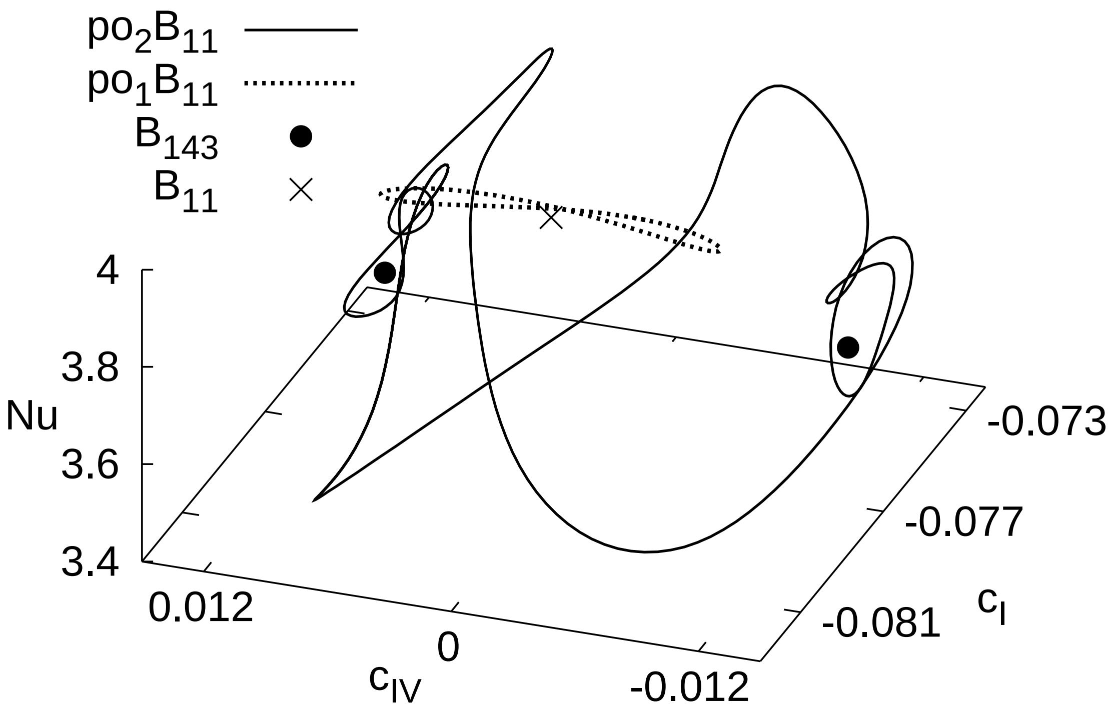

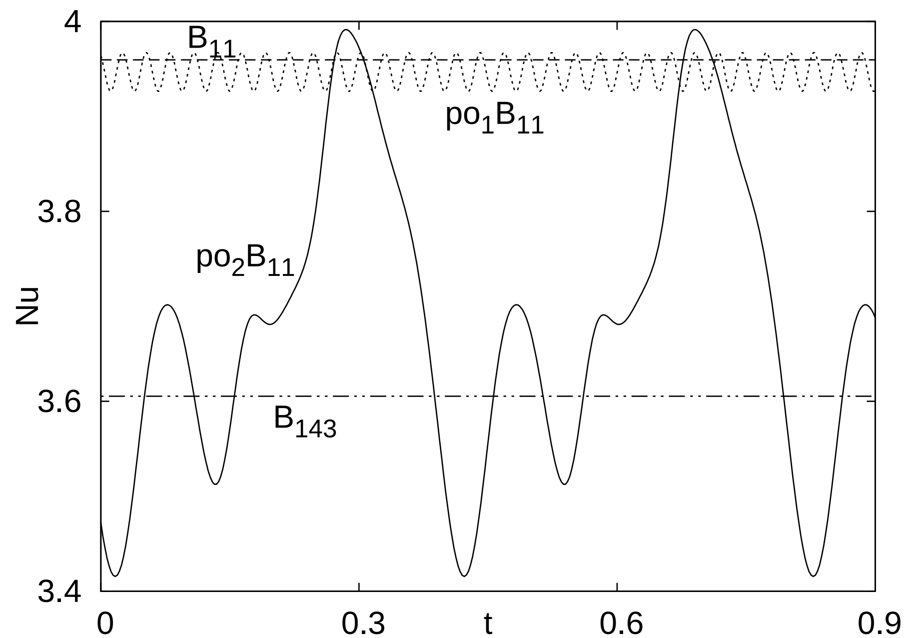

An example with **several orbits**.

Left: po_2B_{11} **at** $Ra = 91\,801.95$ after 4^{th} turning point, close to the **last computed** point . We show also S_y–symmetric solutions: po_1B_{11}**,** B_{11} and two S_y–symmetrically related B_{143}. They are involved in **heteroclinic connections**.

Right: **Evolution with time of the Nüsselt number**.

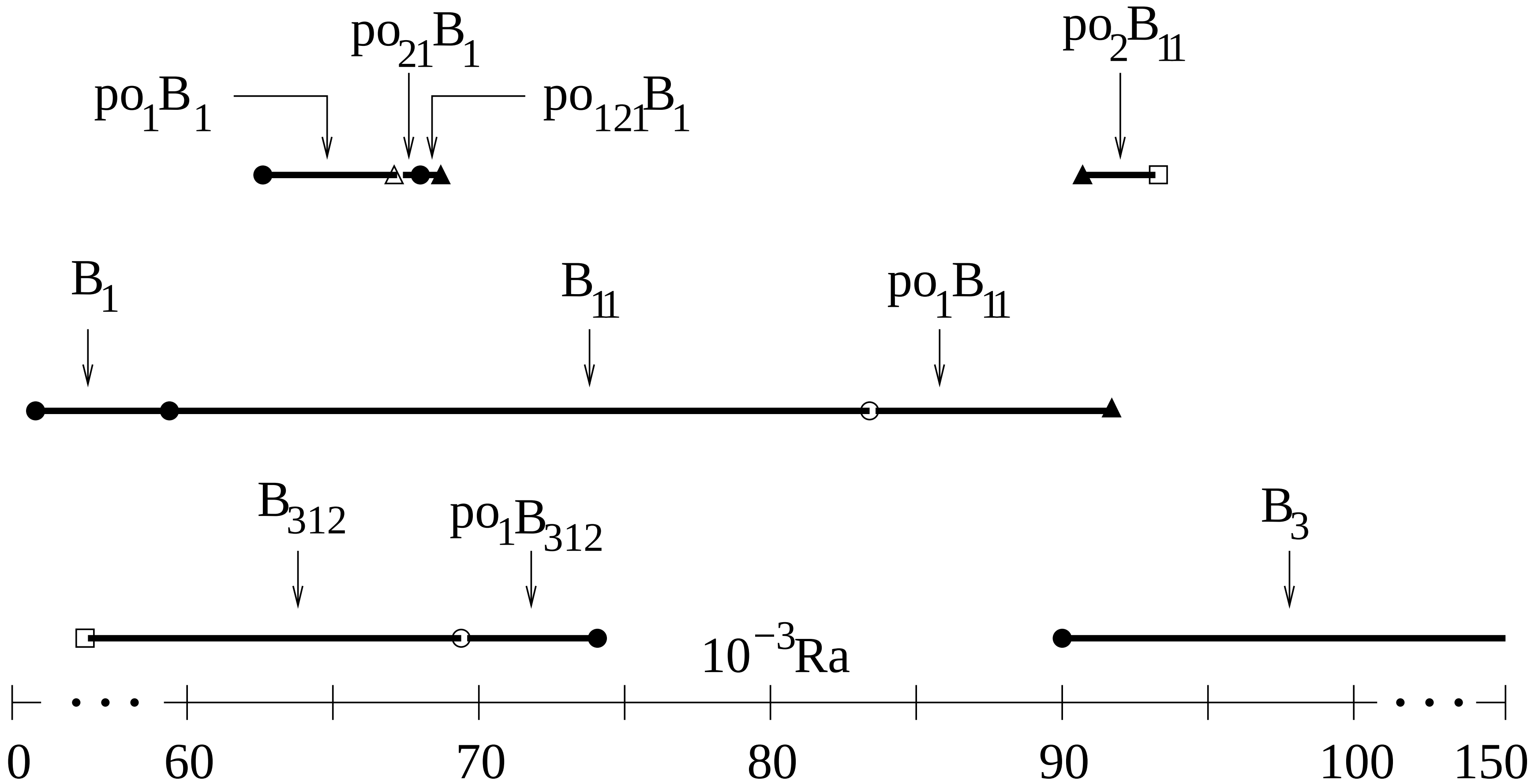

Sketch of the **ranges of stability** of all the stable **identified** solutions. Each solution is stable within the **Rayleigh range** represented by the segment delimited by two bifurcation symbols. **Exchange of stability** between solutions is represented by **adjacent segments** in the sketch. For clarity the scale in the horizontal axis is **magnified in the interval** $[60, 100]$.

Note that **in the full range** there is always a **stable steady or p.o.**

Chaotic dynamics at $Pr = 0.71$

Chaotic dynamics has been found for $Ra < 10^5$ for $Pr = 0.71, 0.75, 0.80$.

A problem: the dynamics for $Pr = 0.71$ has been found to be **chaotic only in** E_7, a non-attracting subspace. **A small initial departure from** E_7 takes the points **away from it**. They are **attracted by** B_{11}, po_1B_{11}**,** po_2B_{11} **or** B_3, depending on the value of Ra (see previous page).

But even **restricted to** E_7 the dynamics is interesting: a **potential strange attractor** is **promoted** to a **true attractor**.

Concretely: **There are different unstable objects (steady and p.o.) in** E_7 **with heteroclinic connections**. This give rise to a strange attractor in E_7. But the orbit **comes close to** po_1B_{312}, attracting (in E_7) in a range ending at Ra_{HC_1} and **it is attracted by it**.

When po_1B_{312} **ends at that** Ra_{HC_1} the **potential attractor** becomes a **true one** (still only in E_7).

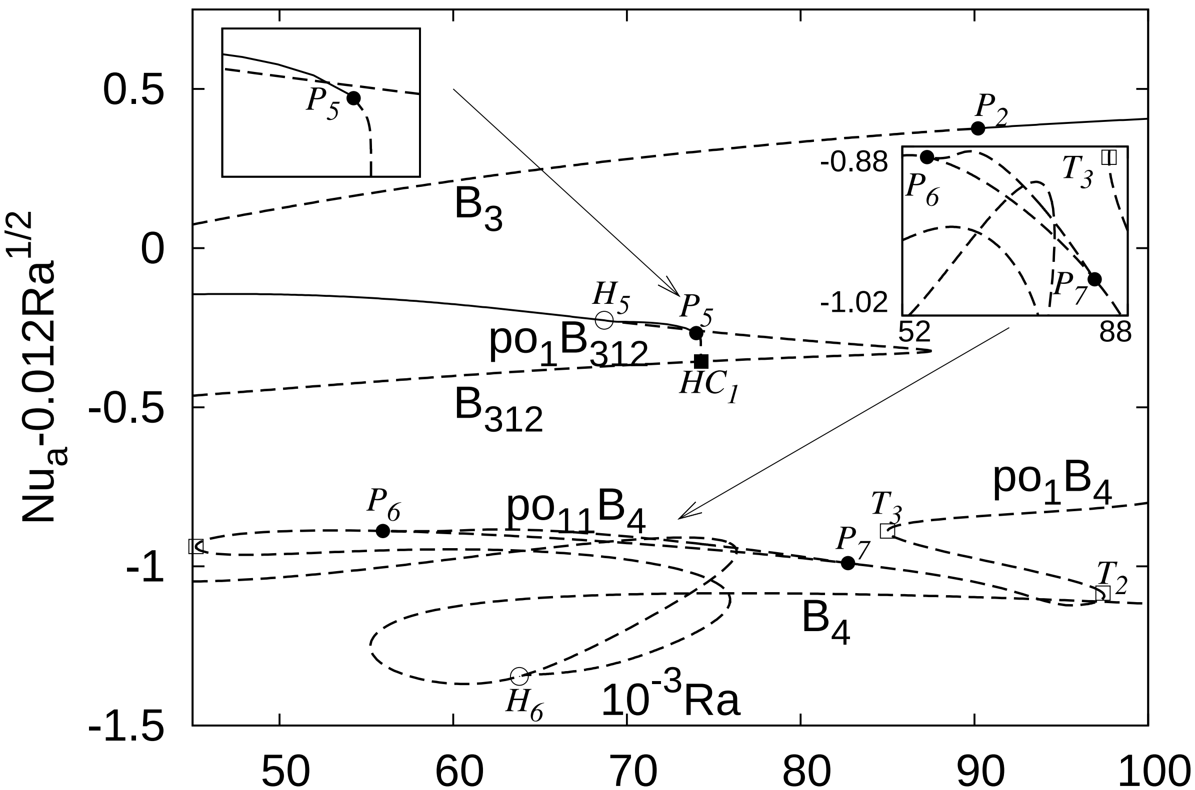

Bifurcation diagram of **steady solutions and periodic orbits** that are related to **chaotic dynamics**.

B_4 has been included to clarify the origin of the po_1B_4.

In contrast, po_1B_{312} **plays a crucial role** in the generation of chaotic dynamics. The initially stable po_1B_{312} **arises at an** H_3 **on** B_{312}. It ends on a **homoclinic** HC_1 ($Ra = Ra_{HC_1} = 74\,256.8441$) with $\lambda_1 = 18.22$, $\lambda_2 = -42.17$ (in E_7) **with** $\sigma = \lambda_1 + \lambda_2 < 0$ (inside E_7) and, hence, **limit of stable p.o.**.

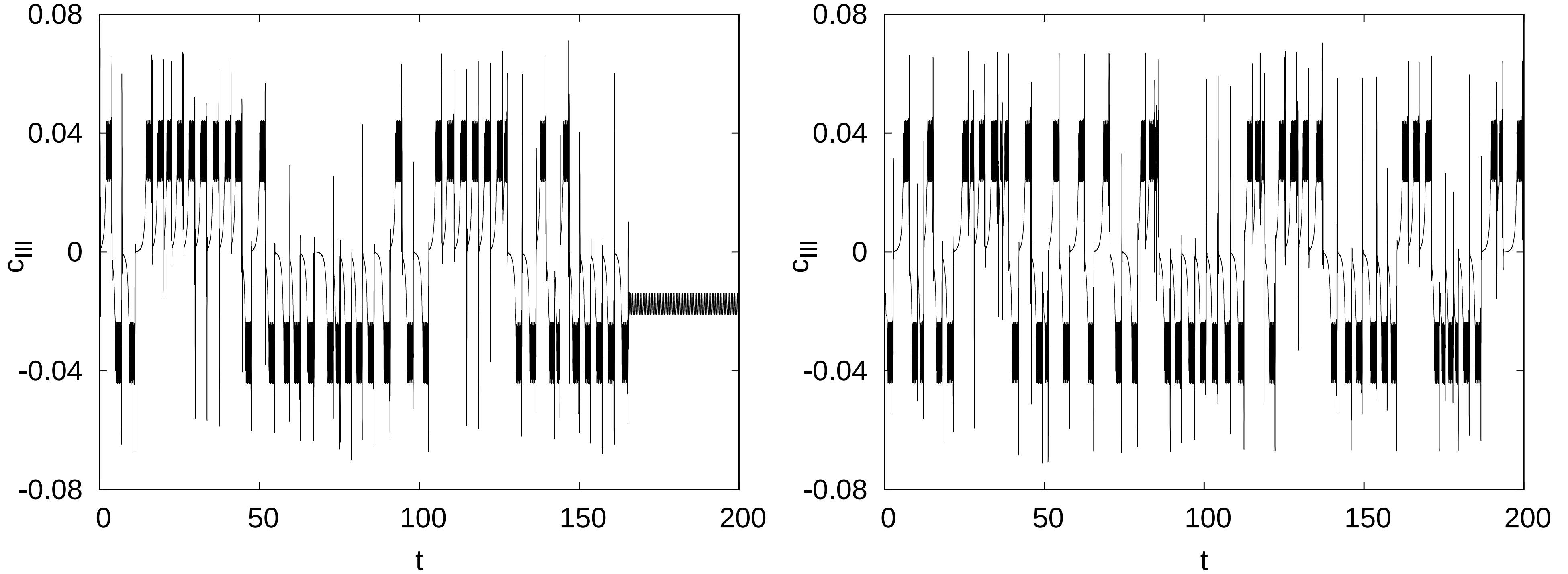

Evolution with time of c_{III}, the first coefficient belonging to the third symmetry block in the truncated expansion. Left: at $Ra = 74\,000 < Ra_h$. Right: at $Ra = 74\,260 > Ra_h$. Note that both Ra are **close to** $Ra_h = Ra_{HC_1}$.

On the left: After a **chaotic transient** the orbit is attracted by a **stable periodic orbit in the** po_1B_{312} **branch**.

On the right: **the p.o. do not longer exists**. The **chaotic behavior persists**.

All these orbits **belong to** E_7.

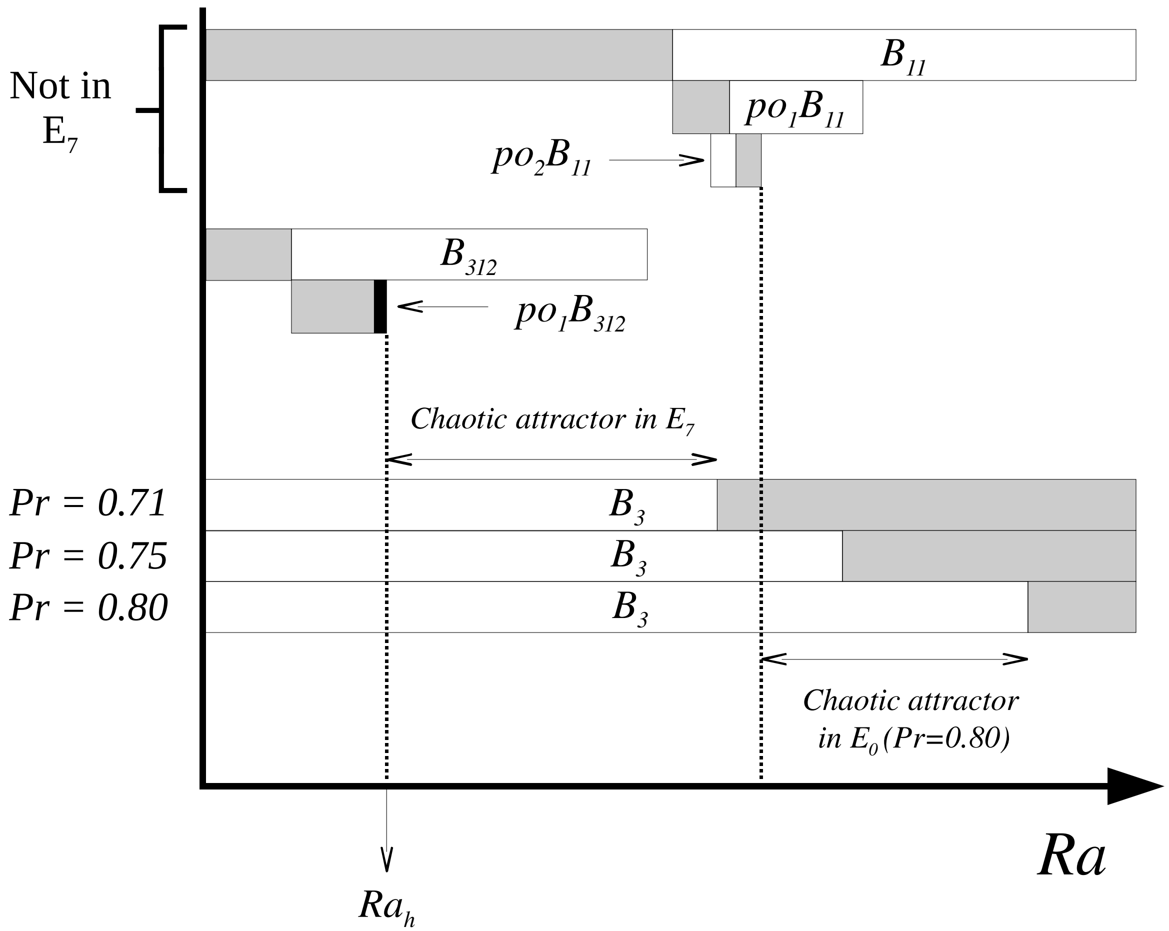

Qualitative sketch of the **ranges of existence and stability** of solutions **relevant** to the occurrence of **chaotic attractors**. **Gray rectangles**: regions where the solutions **attract in the full space E_0**. **Black rectangles** regions where the solutions **attract only in E_7**. **Empty rectangles**: regions with solutions **not attracting neither in E_0 nor in E_7**.

In particular, the **dependence** of the ranges of existence of chaotic attractors **as a function of Pr is shown**.

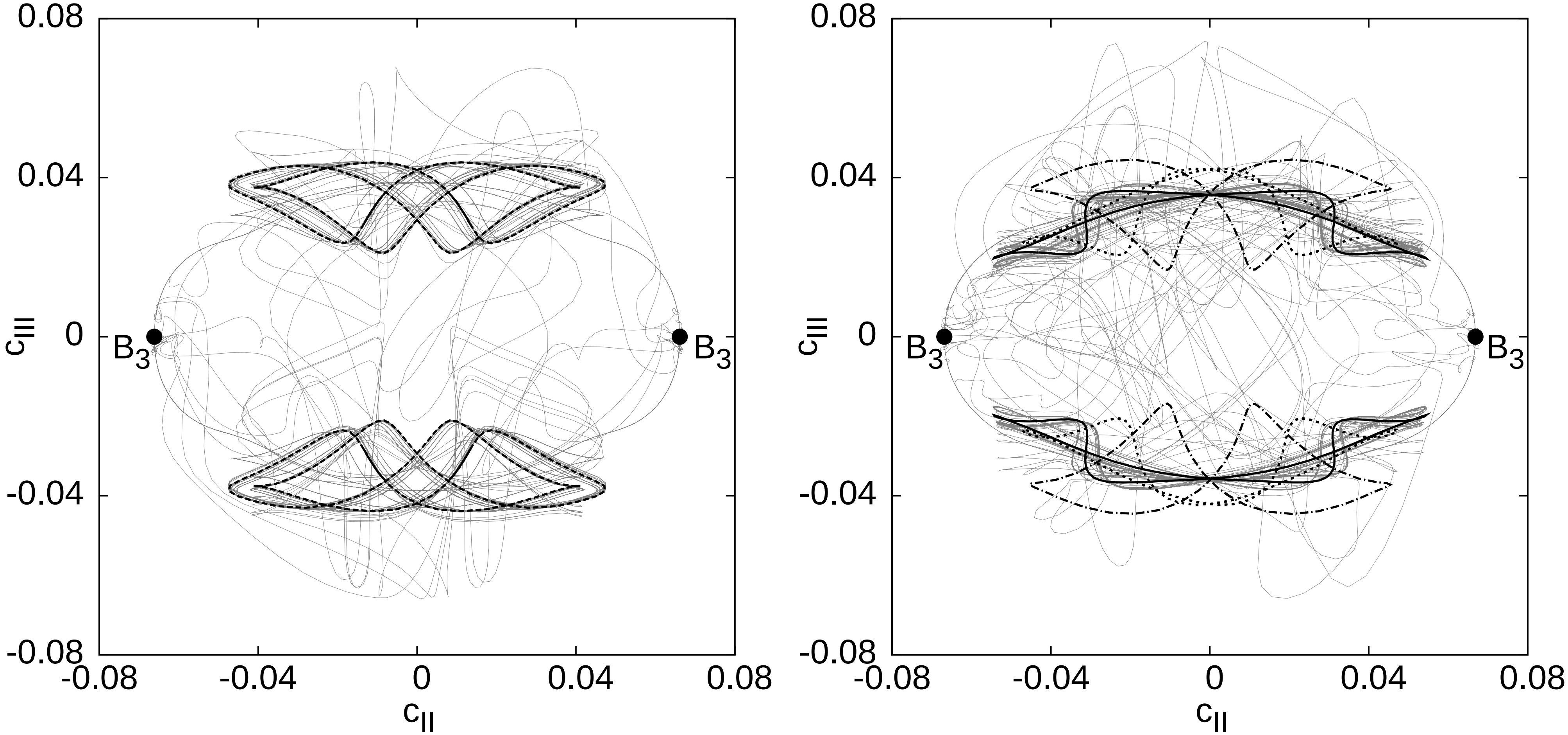

Projection on (c_{II}, c_{III}) of the **chaotic dynamics (attractor only in E_7)** and involved solutions at $Ra = 8 \times 10^4$ (left) and $Ra = 9 \times 10^4$ (right). Attractor in **solid gray lines**. The two symmetric B_3 with **filled circles**. On the left 4 copies (by symmetries) of $po_{11}B_4$ in **dashed black lines**. On the right several orbits of the family po_1B_4 in **solid, dotted and dot–dashed black lines**.

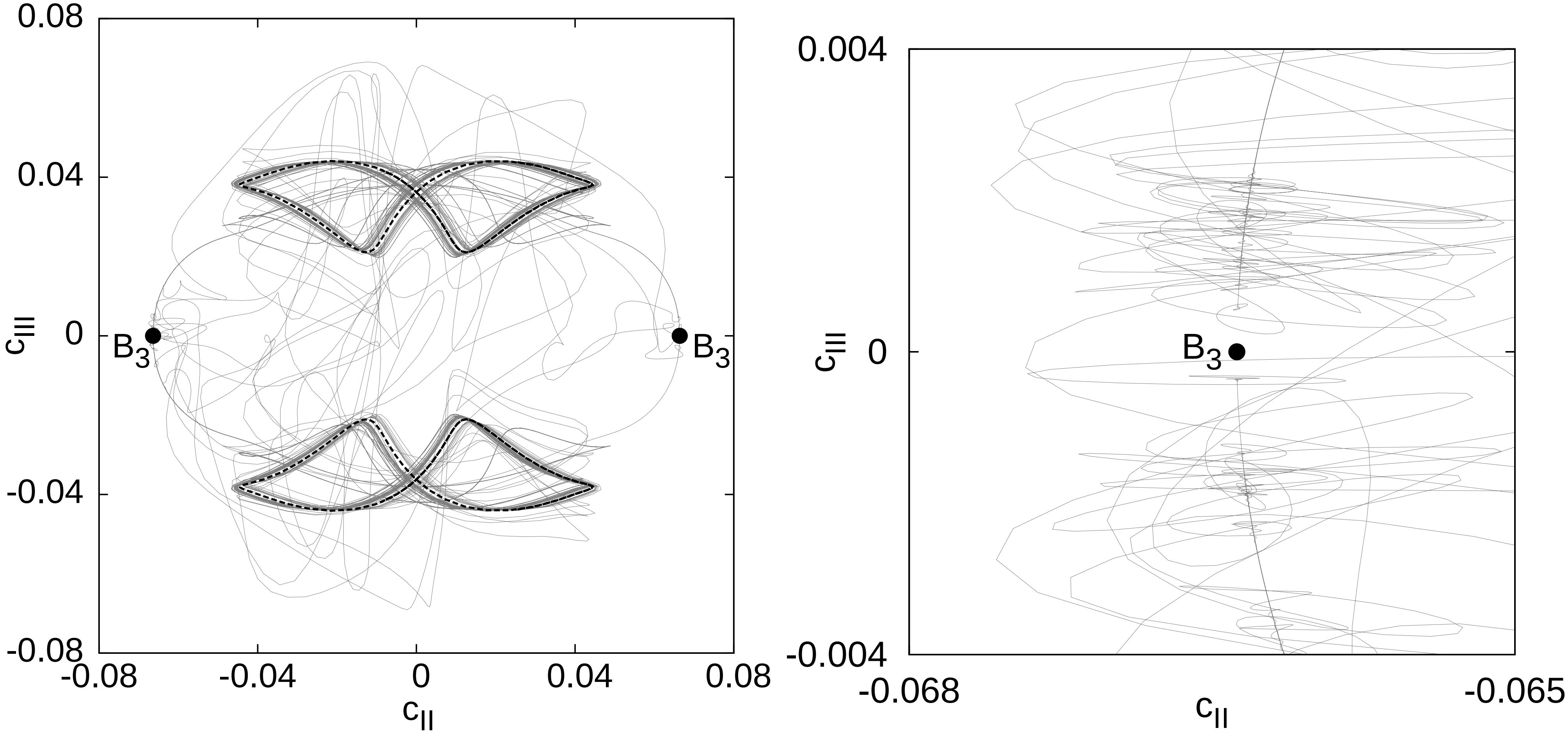

Similar to previous plot for $Ra = 8.3 \times 10^4$ (left) and a **magnification** (right). Attractor (inside E_7) in **solid gray lines**. Two symmetrically related po_1B_4 in **solid black lines**.

Note that, similar to the previous plots, **the orbit in the attractor** remains for a long time **close to the po_1B_4 orbits**, which are mildly unstable.

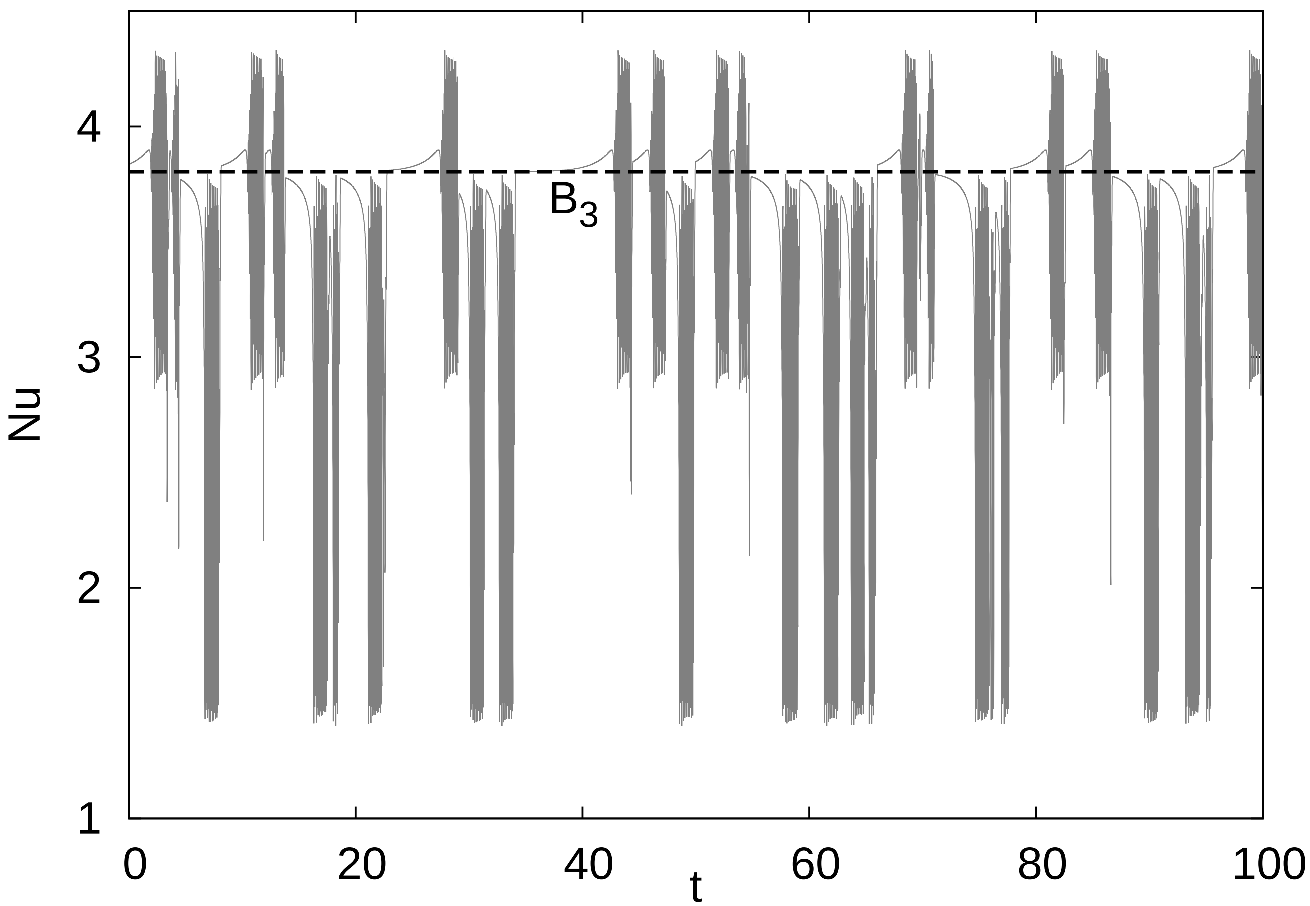

Evolution with time of the Nüsselt number for the **chaotic attractor (in E_7)** at $Ra = 8.3 \times 10^4$. The dashed horizontal line shows the Nu **value** corresponding to the B_3 **solution**.

Departure from E_7 leads the dynamics **to be attracted by** B_3.

But we know from previous work that B_3 **becomes stable for increasing values of** Ra **if** Pr **increases**. See the sketch page. **This suggests...**

Chaotic attractors at $Pr = 0.75$ and $Pr = 0.80$

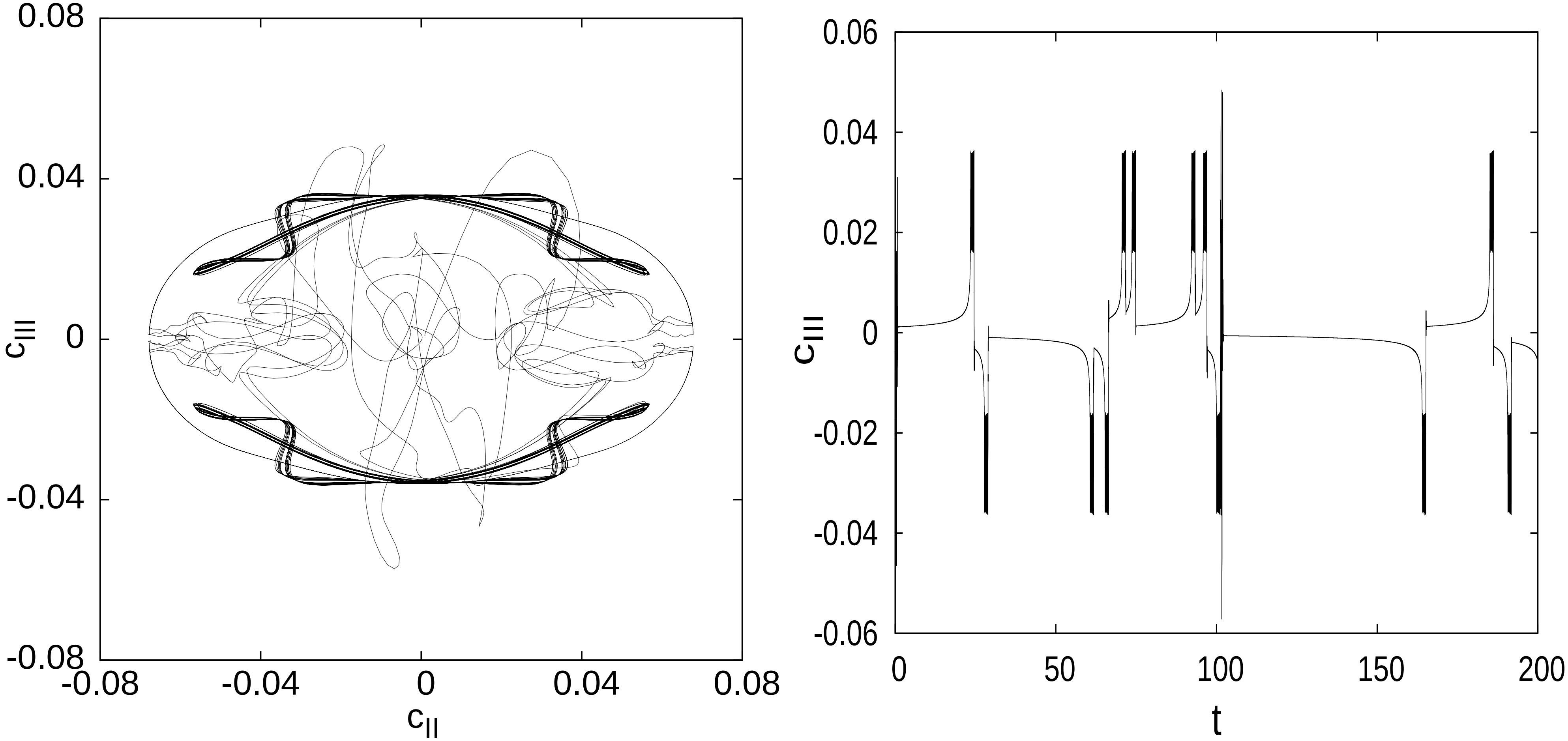

Projection and time evolution of the chaotic attractor at $Ra = 9.5 \times 10^4$ and $Pr = 0.75$.

For these values **all the steady and periodic solutions** that have been found are **unstable**.

Checked for long time intervals (several thousands of units), for **many random initial conditions** and **different space discretisations** (coarser and finer) and by computing **Lyapunov exponents**.

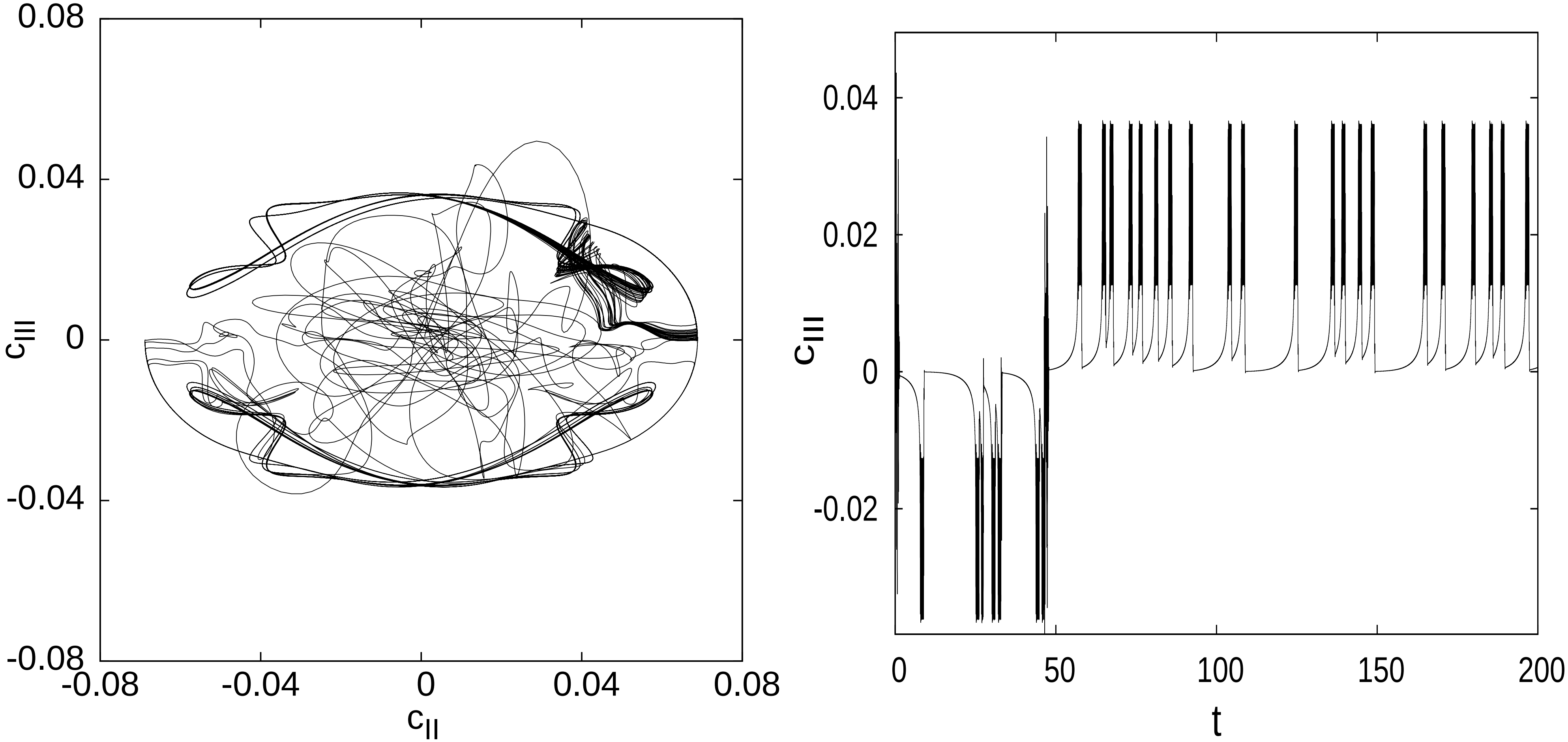

Projection and time evolution of the chaotic attractor at $Ra = 10^5$ **and** $Pr = 0.80$.

For these values **all the steady and periodic solutions** that have been found are **unstable**.

Checked for long time intervals (several thousands of units), for **many random initial conditions** and **different space discretisations** (coarser and finer) and by computing **Lyapunov exponents**.

Thanks for your attention!

And sorry for changing from **DANCE** to **DNASC**:

Dynamics, Nonlinearity, Attractors, Stability and Chaos